Spectroscopic Characterization of Acidity in Chabazite

Brent A. Aufdembrink,† Douglas P. Dee, Paula L. McDaniel, Thomas Mebrahtu,* and Terry L. Slager

Corporate Research Services Department, Air Products and Chemicals, Inc., 7201 Hamilton Boulevard, Allentown, Pennsylvania 18195-1501

Received: October 8, 2002; In Final Form: June 10, 2003

Acid sites in potassium-containing chabazite catalysts, under evaluation for methylamines synthesis, were characterized by thermogravimetric analysis−infrared spectroscopy (TGA−IR), solid state magic angle spinning nuclear magnetic resonance (MAS NMR), and diffuse reflectance infrared Fourier transform spectroscopy (DRIFTS). Spectroscopic results of samples activated between 350 and 650 °C indicate the presence of three distinguishable acid sites: (i) eight-ring Brønsted sites (high-frequency hydroxyls or HF OH), (ii) six-ring Brønsted sites (low-frequency hydroxyls or LF OH), and (iii) nonframework (pentacoordinate and octahedral) AlOH sites. The six-ring/LF OH sites desorb ammonia first with increasing temperature and appear to dealuminate before the eight-ring/HF OH sites. Potassium cation content was found to affect the stability of Brønsted acid sites toward dealumination. Improved catalytic activity and selectivity toward reduced trimethylamine yield, in favor of mono- and dimethylamine, is shown to be a result of optimizing potassium cation content and activation temperature.

1. Introduction

Methylamines are commercially produced by the reaction of methanol and ammonia over an amorphous silica−alumina catalyst.[1,2] Among the three amines produced (mono-, di-, and trimethylamine, or MMA, DMA, and TMA), DMA has the highest market demand whereas TMA has the lowest. The amination reactions, run to equilibrium distribution in a large excess of ammonia, produce large quantities of TMA. As a result, excess TMA and ammonia need to be recycled to increase production of DMA. Over the past decade, shape-selective zeolites have been investigated for improved selectivity (reduced TMA yield) in methylamine synthesis.[3−7] In particular, synthetic chabazite catalysts have been shown to preferentially form MMA and DMA; through variations in zeolite synthesis and activation, TMA selectivity can be varied from 1 to 40%, and DMA selectivity can be increased to greater than 60%.[3] In their patent, Wilhelm et al. demonstrated that sodium- and potassium-exchanged chabazites are highly active and selective for methylamine synthesis.

Corbin's review[2] of zeolite catalysts suitable for methylamine synthesis showed that chabazite and mordenite offer greater selectivity toward MMA and DMA, with <10% TMA yield. In comparison, other zeolites lead to TMA yields as high as 95%. The present study was initiated in an effort to better understand the role of potassium cation content and catalyst activation temperature on zeolite stability and overall catalyst performance. A series of partially potassium-exchanged chabazite samples were selected to gain insight into the role of zeolitic acid sites on catalyst activity and selectivity.

The structure of chabazite consists of double six-rings linked together by tilted four-rings, providing a framework with large cavities that are accessible via eight-ring openings (see Figure 1 for a partial view of a structural model). Previous studies of various forms of ion-exchanged chabazite show that cations may be located (i) at the center or face of double six-rings and (ii) near eight-ring openings or inside the large cavities.[8] The cation sites in chabazite, after NH_4^+ exchange and subsequent calcinations of the zeolite, represent potential acid sites for methylamines synthesis. This work attempts to build on previous characterization work on chabazite and related structures[9−14] and to develop a better understanding of acid site stabilization in chabazite catalysts. Toward this end, a combination of complementary analytical techniques (TGA−IR, NMR, FTIR) was selected to probe the acidity of potassium-exchanged chabazites. Infrared and NMR studies have previously shown that hydrogen-form zeolites exhibit Brønsted sites or bridging hydroxyls whose OH stretching frequencies and chemical shifts depend on the width of the pore hosting the OH species.[14−21] In faujasites or ZSM-20, acid sites located in supercage locations show a high-frequency (HF) band at ∼3630−3650 cm^{-1}; in comparison, acid sites in the smaller sodalite units or hexagonal prisms show a low-frequency (LF) band at 3550−3580 cm^{-1}.[22] In the case of chabazite, the HF and LF bands were assigned to eight-ring and six-ring Brønsted sites, respectively.[15]

More recent work by Cheetham[9,10] and Sauer[23] report experimental and computational studies of chabazite and related structures. In these studies, several framework oxygen positions (O4, O2, O1) were examined for bond lengths, angles, and acid site strengths using probe molecules and computer modeling. The work on HSAPO-34 suggested that the IR band known as HF OH corresponds to the O4 site. This work is focused on monitoring the effect of potassium cation content and activation temperature on chabazite acid sites in the context of methylamine synthesis.

Over the past decade, ^1H NMR spectroscopy has been increasingly used in zeolite acidity studies.[24−28] As will be evident in this report, FTIR and ^1H NMR present a powerful combination of spectroscopic techniques to provide detailed

* Corresponding author. E-mail: mebraht@apci.com.
† Present address: Cargill Central Research, P.O. Box 5699, Minneapolis, MN 55440-5699.

10.1021/jp027163p CCC: $25.00
Published on Web 08/23/2003

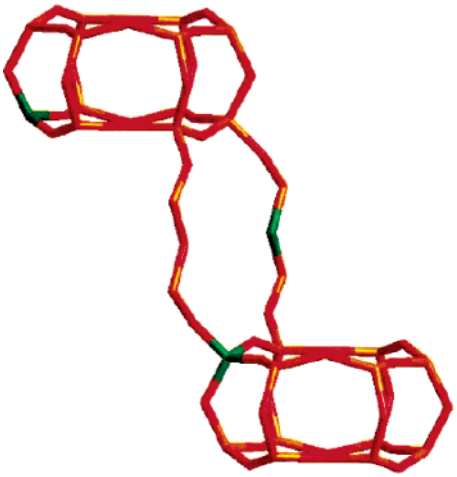

Figure 1. Representation of Chabazite structure, illustrating two double six-rings and an eight-ring opening.

TABLE 1: Elemental Analyses of As-Synthesized and Ammonium-Exchanged Chabazite Samples

sample	no. of exchanges	Si/Al	K/Al	wt % K_2O
CHA	NA (as-synthesized)	2.04	0.98	20.4
CHA-1	1	2.04	0.28	6.91
CHA-2	2	2.04	0.13	3.19
CHA-3	3	2.04	0.06	1.49
CHA-4	4	2.03	0.04	0.77

characterization of acid sites in zeolites and related materials. Haw[29] has recently reviewed the use of probe molecules and NMR spectroscopy to study the relative acid site strength. The impact of CO or other probe molecules on shifts in the IR frequencies of HF and LF OH sites in chabazite provides insight into the relative acid site strengths of the two types of Bronsted sites.[9]

2. Experimental Section

Synthesis of Chabazite. Chabazite was prepared by conversion of calcined NH_4^+-Y (UOP LZ-Y64) as described in US Patent 4,925,460.[30] Analysis by X-ray fluorescence of base-treated (2 M KOH, 8 h) showed 55.3% SiO_2, 22.9% Al_2O_3, 20.4% K_2O, corresponding to the following molar ratios: Si/Al = 2.05, K/Al = 0.98. The base-treated sample was treated with 2 M $(NH_4)_2SO_4$ at 100 °C for 2 h. Approximately one-fourth of the sample was removed from the preparation and the exchange was repeated on the remaining portion of the sample. Each aliquot of the sample was washed with DI water and dried at 110 °C. This sequence produced samples that had been exchanged one to four times with ammonium sulfate. Assuming that no dealumination occurs during exchange, the K/Al ratio indicates the percent of cation exchange for each of the materials. Elemental analyses of the exchanged samples are summarized in Table 1. Samples were analyzed in the as-synthesized form, and after activation in flowing air at 350, 450, 550, or 650 °C for 2 h. After activation, the samples were allowed to equilibrate with the atmosphere. For some analyses, drying was necessary to remove re-adsorbed water.

Characterization of Chabazite. Prior to analysis, care was taken when dehydrating chabazite samples because extended periods of heating or high temperatures may cause changes to the distribution among HF OH, LF OH, and AlOH species.

TGA−IR. Prior to analysis by thermogravimetric analysis−infrared spectroscopy (TGA−IR), samples were purged at 25 °C for at least 10 min to eliminate H_2O and CO_2 in the gas lines. TGA−IR analyses were performed on a TA Instruments 2050 TGA by ramping the temperature at 10 °C/min to 850 °C in 100 cm^3/min N_2. In this experiment, the evolved gases are passed through a 10 cm IR gas cell from ICL. The IR spectrum was collected at 4 cm^{-1} resolution and a gain of 1 on a MIDAC IR. The spectra were collected as a series of 32 co-added spectra at 1 min intervals. Profiles of the evolved gases were prepared by measuring the IR absorbance for H_2O (1652.7 cm^{-1}) and NH_3 (965 cm^{-1}). Using these profiles the wt % NH_3 or H_2O was determined by integrating the peak areas for the profile of the gas-phase bands, multiplying by a calibration factor and dividing by the sample weight.

Solid State MAS NMR. ^{29}Si MAS NMR spectra of hydrated samples were obtained using a Bruker ASX-200 FT-NMR spectrometer equipped with a magic-angle-spinning multinuclear probe (Bruker Instruments) tuned to 39.756 MHz. The crushed samples (approximately 0.3 g each) were spun in zirconia rotors at 3 kHz. TMS was used as an external chemical-shift reference. To ensure quantitative conditions, an 8 s relaxation delay and a 45° flip angle were used to collect approximately 3000 scans for each spectrum. Line broadening (40 Hz) was applied to improve signal-to-noise ratios. Resonances in the ^{29}Si MAS NMR spectrum were deconvoluted into individual line shapes with mixed Gaussian/Lorentzian character and assigned to Si(4Al), Si(3Al), Si(2Al), Si(1Al), and Si(0Al) environments that are well established in the literature for zeolites.[31]

^{27}Al MAS NMR spectra of hydrated samples were obtained using a Bruker AM-500 FTNMR spectrometer equipped with a magic-angle-spinning multinuclear probe (Doty Scientific) tuned to 130.32 MHz. The crushed samples (approximately 30−60 mg) were spun in zirconia rotors at 11 kHz to keep the spinning sideband intensity of the tetrahedral resonance (50−60 ppm) from overlapping with any octahedral resonance (~0 ppm).[31] $Al^{3+}\cdot 6H_2O$ was used as an external chemical-shift reference and was prepared by dissolving an aluminum salt in water. Acquisition conditions involved the use of a 1 s relaxation delay and 1 ms observe pulse, corresponding roughly to a 10−15° pulse angle. Although these conditions should be quantitative for visible aluminum, the possibility exists that some aluminum in a highly asymmetric environment is undetected due to quadrupole broadening not adequately reduced by MAS and high field. An additional cause for loss of aluminum signal is inadequate sample hydration, which can result in under-representation of nonframework (octahedral) aluminum species. ^{27}Al MAS NMR spectra were processed using 40−100 Hz line broadening depending on the signal-to-noise of the original data.

All ^{1}H NMR experiments were performed at room temperature using a Bruker AM-500 FT-NMR spectrometer equipped with a magic-angle-spinning multinuclear probe (Doty Scientific) tuned to 500.13 MHz. The samples were spun in zirconia rotors at 10 kHz. Calcium hydroxy apatite was used as an external chemical-shift reference and for spin counting. A receiver gain of 8 and 300 scans were used to acquire each spectrum; all other parameters, including the pulse sequence cycle times, were standard. No additional line broadening was necessary.

Except where noted, the samples were crushed and then dried at 400 °C (1 °/min ramp and then held at the temperature until the background pressure dropped to below 0.01 mTorr) prior to ^{1}H MAS NMR experiments. Samples that were dried at a lower temperature were held at the temperature for approximately 30 h. After the samples were dried, approximately 30−50 mg was transferred in an argon glovebox to the NMR

rotors. Extra care was taken to prevent exposure of the dried samples to water vapor.

Phase and baseline corrections, as well as integration, were performed on the spectral region between +15 and −5 ppm. Spectral deconvolution was performed using *GLINFIT.3004*, which provides only semiquantitative results. Purely Gaussian character of the component peaks was assumed. In fitting a typical spectrum to the six possible peaks, it was necessary to include two additional peaks, one centered between the 6.4 and 4.4 ppm peaks and another between the 3.7 and 2.5 ppm peaks; it is likely that these additional peaks would be unnecessary if a combination of Gaussian and Lorentzian character were incorporated into the component peaks. Contributions from the small areas associated with these two additional peaks were evenly assigned to the neighboring components.

DRIFTS. All IR spectra were collected using a Harrick diffuse reflectance attachment housed in a Nicolet Magna 750 infrared spectrometer with a mercury cadmium telluride (MCT) detector cooled to −196 °C. Samples were loaded in a Harrick HVC-DRP DRIFTS cell having KBr windows. This cell can be operated at controlled temperatures from room temperature up to 600 °C and at atmospheric pressure using N_2 at a flow rate of 10 cm^3/min. The cell was loaded with approximately 50 mg of zeolite. All spectra presented here were collected at 28 °C.

Sample spectra are presented as a ratio of the raw spectrum obtained under N_2 to that of KBr obtained after heating to 100 °C in flowing N_2. Spectra were collected by summing 500 scans for the sample or the background spectra using 0.5 cm^{-1} resolution (one data point every 0.25 cm^{-1}). The standard treatment in the IR cell was to heat the sample in flowing N_2 at 10 cm^3/min at the desired temperature for 1 h. After treatment, samples were cooled to room temperature prior to data collection.

DRIFTS spectra are displayed using the log(1/*R*) format. Because DRIFTS is a scattering technique, the signal levels are dependent on the scattering coefficient, which is strongly dependent on the particle size and degree of packing of the sample. For this reason, only qualitative comparisons based on band intensities were made from one sample to another. However, quantitative comparisons of different heat treatments on the same sample preparations are valid and trends in the intensity changes allow comparison among the spectra.

Evaluation of Chabazite Catalyst Performance.[3] Catalyst activity was evaluated in a plug flow reactor. Feeds to the reactor were delivered by ISCO syringe pumps, which were operated by flow controllers to within 0.01 cm^3/h. The catalyst extrudates were charged to a $^1/_2$ in. i.d. stainless steel tube. Reactions were performed at 275 °C under the following conditions: 250 psig, ammonia/methanol (N/R) ratio of 3.5, GHSV = 1000 h^{-1}. Effluent from the reactor was passed through a Valco 4-port sampling valve and a back-pressure regulator. Sampling was done on a liquid phase for consistency; samples were injected hourly to a Hewlett-Packard 5890 GC.

3. Results and Discussion

TGA analysis with simultaneous IR detection of the evolved gases was performed on a series of samples to study the effects of activation temperature and potassium cation loading. Figure 2 of a nonactivated sample (CHA-4) shows two primary weight loss regions. On-line detection of evolved gases by FTIR allows the unambiguous identification of species that contribute to the observed weight losses. This figure clearly demonstrates that NH_3 evolution is completed in two steps and that the low-temperature component overlaps with desorption of physisorbed and chemisorbed H_2O. There is also a smaller H_2O desorption peak that overlaps with the high-temperature NH_3 peak. This water loss is most likely associated with zeolite dehydroxylation and/or dealumination. The data clearly demonstrate that the two primary weight loss regions are composed of four separate desorption peaks, which are assigned as follows: (i) adsorbed H_2O (<250 °C), (ii) weakly bound NH_3 (200−300 °C), (iii) strongly bound NH_3 (300−550 °C), and (iv) structural H_2O loss (400−550 °C) due to zeolite dehydroxylation and/or dealumination. The band shape for the NH_3 profile shows some asymmetry, indicating heterogeneity of the acid sites. Table 2 summarizes the data for the TGA, H_2O, and NH_3 weight losses as a function of activation temperature.

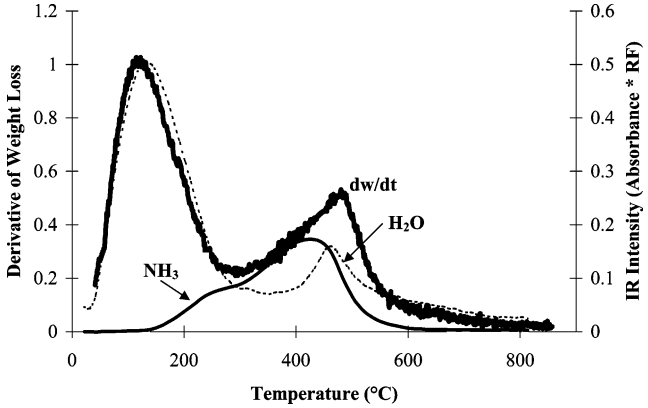

Figure 2. Comparison of IR vapor phase signals for desorbed H_2O and NH_3 with the derivative of the weight loss from TGA analysis for nonactivated chabazite (CHA-4).

The sum of the weight of H_2O and NH_3 calculated from the IR signals is similar to the weight losses seen by TGA. It is interesting to note that approximately the same amount of structural water (∼2−3 wt %) is evolved in all of the samples. With increasing activation temperature, there is an increase in the onset temperature at which dehydroxylation begins to occur. This suggests that higher activation temperatures impart increased stability to the zeolite structure. At activation temperatures greater than 550 °C, no more high-temperature H_2O is released, indicating that the CHA structure has collapsed. The low-temperature NH_3 release is gone at activation temperatures >350 °C, and as expected, the amount of high-temperature NH_3 retained decreases with increasing activation temperature.

Figure 3 presents ^{29}Si MAS NMR results of chabazite (CHA-4) activated at 350−650 °C. Deconvolution of the spectra[31] indicated Si/Al ratios increased from 2.2 to >5.0 with increasing activation temperature. These results suggest significant levels of dealumination upon activation at the higher temperatures.

^{27}Al NMR MAS results (Figure 4) of the same series of samples confirm dealumination with increased activation temperature; dealumination is noted through the increasing contribution of pentacoordinate (P) and octahedral (O) aluminum. The sample activated at 350 °C showed a major signal at ∼60 ppm, indicating the presence of primarily tetrahedral Al (T). Resonances centered at 30 ppm (P) and 0 ppm (O) indicate increased dealumination with increased activation temperature. The nature of pentacoordinate Al, although categorized here as nonframework, may be better described as a dangling, partially attached aluminum species, whereas octahedral Al totally disassociates from the framework. The assignment of pentacoordinate as framework-attached is partly supported by a shoulder at 40−50 ppm attributed to a true tetrahedral framework species perturbed by a nonframework cation that appears as a broad

TABLE 2: TGA−IR Data, Including Water and Ammonia Weight Loss Measurements, for Unactivated and Activated (350−650 °C) CHA-4

		H_2O wt. loss (%)			NH_3 wt loss (%)		
sample	activation temp, °C	low *T* (°C)	high *T* (°C)	total	low *T* (°C)	high *T* (°C)	total
CHA-4	none	**13.6** (190)	**2.2** (451)	**15.8**	**2.7** (283)	**5.0** (421)	7.7
CHA-4	350	**9.5** (190)	**1.8** (511)	**11.3**	0	**4.8** (488)	4.8
CHA-4	450	**2.1** (190)	**2.8** (594)	**4.9**	0	**2.6** (551)	2.6
CHA-4	550	**8.5** (190)	**2.2** (690)	**10.7**	0	**0.02** (666)	0
CHA-4	650	**8.9** (190)	**0**	**8.9**	0	**0**	0

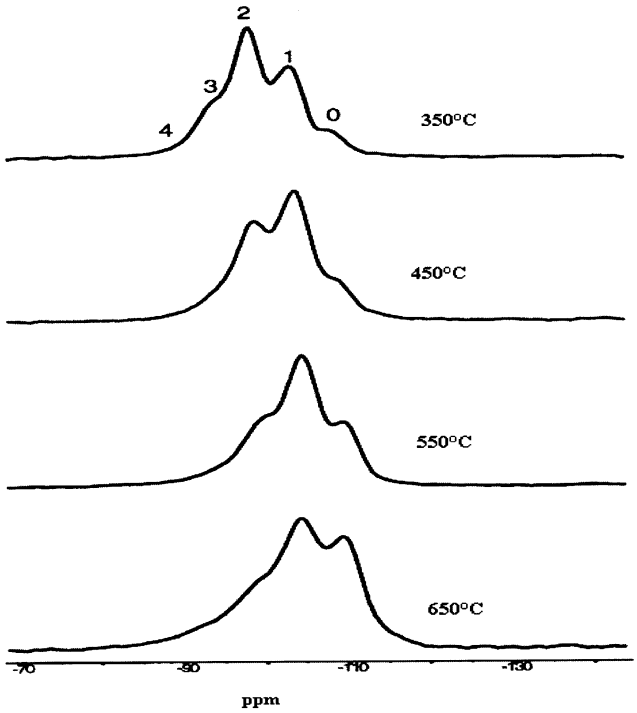

Figure 3. ^{29}Si MAS NMR of CHA-4, indicating increasing levels of dealumination at the higher activation temperatures: 0 = Si(0Al); 1 = Si(1Al), 2 = Si(2Al); 3 = Si(3Al); 4 = Si(4Al).

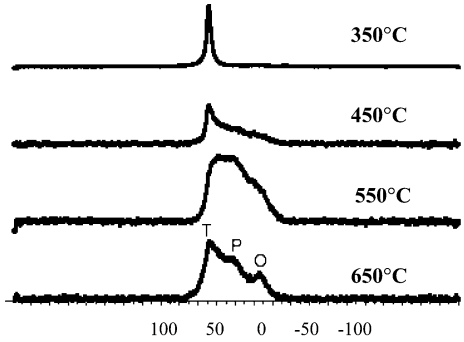

Figure 4. ^{27}Al MAS NMR of CHA-4, indicating increasing levels of dealumination at the higher activation temperatures (T = tetrahedral, P = penta-cordinated, O = octahedral).

upfield shoulder on the main tetrahedral.[32] This feature's growth appears to be linked to the emergence of the pentacoordinate species. Further, its broadened line width is indicative of the strain or lower symmetry that these tetrahedral environments would experience when adjacent to pentacoordinate/nonframework aluminum species.

Closer examination of the series shown in Figure 4 shows that although the general trend is increased nonframework aluminum with activation temperatures of 450 °C and greater, there appears to be a diminished amount of pentacoordinate species at the highest temperatures. Because the ^{29}Si MAS NMR results for the 650 °C activated material confirm further dealumination, it is likely that some of the nonframework aluminum species are not detected due to extensive line-broadening. Aluminum can become invisible to detection using routine MAS NMR acquisition conditions if the environment around the aluminum becomes significantly asymmetric.

TABLE 3: IR and ^{1}H NMR Peak Assignments for Chabazite Zeolites

functional group	IR frequency, cm^{-1}	^{1}H NMR chemical shift, ppm
SiOH (terminal)	3747	0.8, 1.9
AlOH (nonframework)	3650	2.6
AlOHSi (HF OH)	3620	3.7
AlOHSi (LF OH)	3570	4.4
NH_4^+ (NH stretch)	3380, 3260	6.4
H_2O (stretch)	3400−3000	

Table 3 summarizes the representative IR frequencies and NMR[31] chemical shifts for different bands present in the spectra of CHA-4 and other chabazite zeolites. The listed values are approximate and vary slightly depending on ion content, catalyst activation, and sample dehydration.

Unactivated Chabazite (CHA-4). Figure 5 shows IR spectra for unactivated chabazite (CHA-4) in the OH and NH stretching region (3900−3100 cm^{-1}) at room temperature and after dehydration at 150 and 250 °C. H_2O and NH_4^+ bands due to bending modes in the 1900−1300 cm^{-1} region (not shown) mirror the changes in the OH region. The spectrum at 25 °C shows broad features due to hydrogen bonding of the physisorbed water in the OH region; this is also confirmed by the H_2O bending mode at 1653 cm^{-1}. Similarly, the ^{1}H NMR spectrum of this sample is dominated by a very broad resonance centered at ∼5.6 ppm, which has been assigned to residual adsorbed water.

During sample dehydration of CHA-4 at 150 °C, physisorbed H_2O is removed. This desorption shifts the H_2O bending mode to 1680 cm^{-1} (chemisorbed H_2O) and splits the NH_4^+ bending mode into two overlapping bands, which have been previously assigned as NH_3 adsorbed on LF and HF OH groups.[33]

Activated Chabazite (CHA-4). Spectra discussed in this section correspond to the fully exchanged chabazite samples that were activated and then dehydrated to remove residual water prior to the IR and NMR experiments. Figure 6 shows the effects of each activation temperature (350, 450, 550, 650 °C) on CHA-4. In general, the NH_4^+ bands in the IR and NMR spectra decrease in intensity with increasing activation temperature. The IR spectrum for the 550 °C activated sample shows the residual NH_3 is mostly adsorbed on the HF OH sites, and an activation temperature of 650 °C is required to completely desorb the ammonia from these HF OH sites.

The desorption of NH_3 with increasing activation temperature is accompanied by the growth of both the LF and HF OH bands in the IR spectra. The HF OH band at 3610 cm^{-1} appears as a shoulder at 350 °C and increases in intensity as the temperature increases, reaching a maximum in definition and intensity at

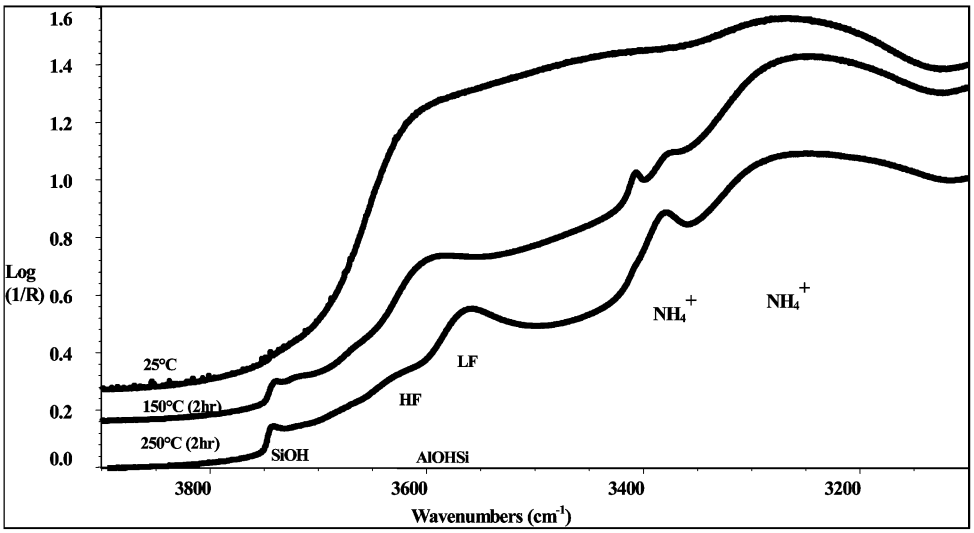

Figure 5. IR spectra of CHA-4, showing increasing levels of dehydration at higher activation temperatures (25, 150, 250 °C).

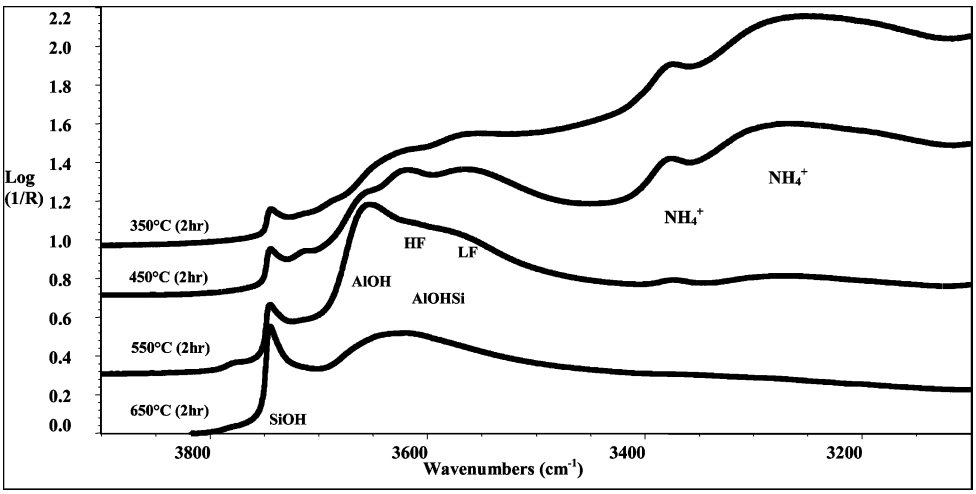

Figure 6. Effect of activation on CHA-4 in the OH spectral region (350, 450, 550, 650 °C).

450 °C. The LF OH band at 3570 cm^{-1}, which initially appeared at 250 °C (Figure 5), remains as a shoulder to the AlOH and HF OH bands at 550 °C.

The formation of nonframework AlOH species can be tracked by monitoring the IR band at 3650 cm^{-1} and the NMR resonance at 2.7 ppm. Initially, this band appears in the IR spectra as a shoulder at 350 °C and continues to increase at 450 and 550 °C. Consistent with increasing framework dealumination, a small band appears at 3780 cm^{-1}, which is assigned to nonframework hydroxyl groups associated with aluminum-containing species. By 650 °C, the AlOH feature at 3650 cm^{-1} loses resolution and blends with the HF OH band.

Figure 7 illustrates the effect of activation temperature on the ^{1}H NMR spectra of CHA-4. The ^{1}H NMR data show that activation leads to ammonia desorption as well as to the formation of two types of Brønsted acid sites (4.4 and 3.7 ppm) and hydroxyls due to nonframework Al (2.6 ppm).[33] Comparing the changes in the NMR signals with the IR signals confirm these assignments. Analogous studies in the literature have shown that zeolite pore width affects OH frequency.[15,22,33] Peak assignments from ^{1}H NMR[33] and IR spectra are consistent with the following acid sites in activated chabazite: (i) eight-ring Brønsted sites (high-frequency hydroxyls or HF OH), (ii) six-ring Brønsted sites (low-frequency hydroxyls or LF OH), and (iii) nonframework AlOH sites.

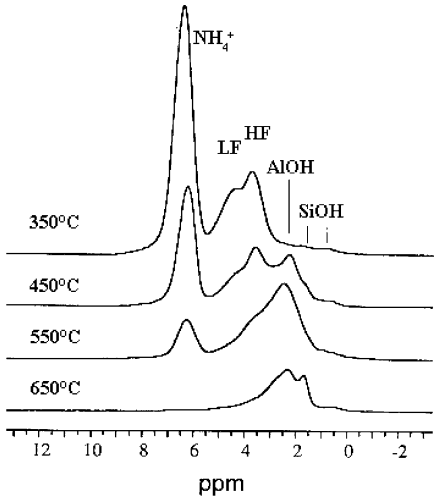

Figure 7. ^{1}H NMR spectra of CHA-4 activated at 350−650 °C.

The effect of the potassium cation levels in chabazite is shown in Figure 8. These spectra compare the OH and NH (3900−3100 cm^{-1}) region for the 550 °C activation treatment. At 550 °C, some NH_4^+ remains in the catalyst. Potassium cations appear to prefer LF OH sites because the HF NH_4^+ band at 1410 cm^{-1} increases in intensity with decreasing K_2O exchange levels. Because the LF OH sites appear to dealuminate first, stability

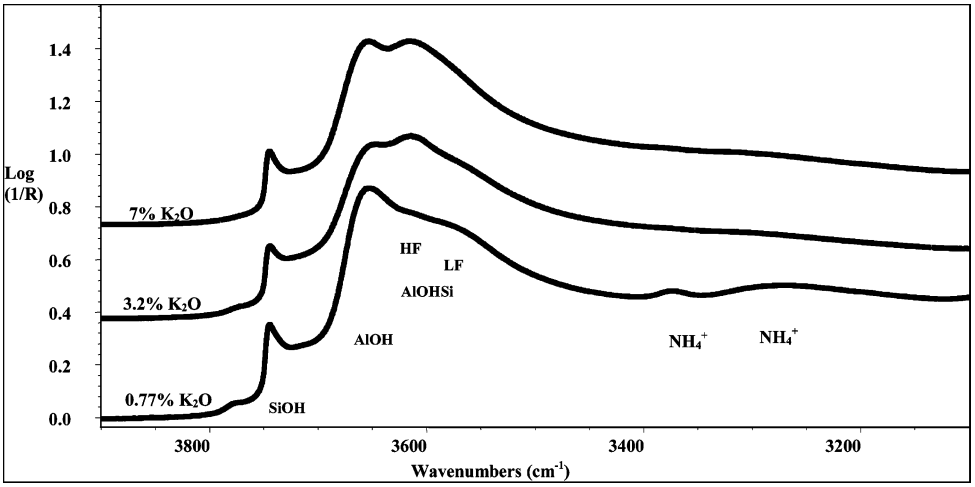

Figure 8. Effect of K_2O on the OH region for 450 °C activation of CHA-1 (7% K_2O), CHA-2 (3.2% K_2O), and CHA-4 (0.77% K_2O).

TABLE 4: TGA−IR Data, Including Water and Ammonia Weight Loss Measurements, for 450 °C Activated Chabazite Zeolites as a Function of K_2O Content

		H_2O wt loss (%)			NH_3 wt loss (%)		
sample	% K_2O	low *T* (°C)	high *T* (°C)	total	low *T* (°C)	high *T* (°C)	total
CHA-1 450 °C	7.0	**1.4** (190)	**2.2** (772)	**3.6**	**0**	**1.2** (490)	1.2
CHA-2 450 °C	3.2	**7.2** (190)	**2.1** (641)	**9.3**	**0**	**1.4** (538)	1.4
CHA-4 450 °C	0.77	**2.1** (190)	**2.8** (594)	**4.9**	**0**	**2.6** (551)	2.6

TABLE 5: Catalyst Performance of Chabazite Catalysts Activated at 450, 550, and 650 °C[a]

sample%	activation temp, °C	methanol conv,[b] %	selectivity, % TMA	DMA	MMA
CHA-1	450	91.7	0.7	40.1	59.2
6.9 wt % K_2O	550	96.0	0.0	44.2	55.8
	650	97.3	0.3	49.3	50.4
CHA-2	450	88.6	2.0	40.5	57.5
3.2 wt % K_2O	550	98.4	0.9	49.6	49.5
	650	81.8	0.1	42.0	57.7
CHA-3	450	87.9	3.0	40.0	57.0
1.5 wt % K_2O	550	95.8	1.0	48.0	51.0
	650	NA	NA	NA	NA
CHA-4	450	92.0	3.0	40.0	57.0
0.77 wt % K_2O	550	99.3	1.0	47.0	52.0
	650	< 80	NA	NA	NA

[a] Reaction temperature = 275 °C, pressure = 250 psig, ammonia/methanol (N/R) = 3.5, GHSV = 1000 h^{-1}. [b] 275 °C, 1000 GHSV, 3.5 N/R.

toward dealumination is offered by higher K^+ levels. This is consistent with ^{29}Si NMR data and stability observed toward high-temperature calcination. The 3780 cm^{-1} band, which is associated with nonframework AlOH, becomes more prominent in the sample with the lowest potassium content.

These samples were also analyzed by TGA/IR. The data are summarized in Table 4. As seen with the activation study, comparable amounts of structural H_2O are desorbed from the samples, although the desorption temperature increases with higher K^+ levels. This suggests that K^+ ions impart increased stability to the zeolite from dehydroxylation and/or dealumination.

Table 5 compares the catalytic activity and selectivity of chabazite catalysts; careful examination of the table shows the lowest selectivity to TMA and optimal activity typically occurs at 550 °C activation. It is interesting to note that, taking into account our spectroscopic results, the most optimal catalysts require both framework and nonframework acid sites to maximize activity (>95% methanol conversion) and selectivity (<1% TMA yield). This is perhaps related to preferred adsorption and reaction sites for the two reactants, methanol and ammonia. The data also suggest that potassium cations and nonframework AlOH sites both contribute toward improved shape selectivity. With the highest activation temperatures (650 °C), the lower potassium content catalysts were not stable enough toward dealumination and did not exhibit acceptable methanol conversion.

4. Conclusions

NH_4^+-exchanged and activated chabazite catalysts were characterized by TGA−IR, DRIFTS, and Solid state MAS NMR (^{27}Al and ^{29}Si). After catalyst activation, these results show the formation of Brønsted acid sites and nonframework (pentacoordinate and octahedral) aluminum. A detailed structural understanding of the acid sites in chabazite catalysts was obtained as a function of K^+ content and activation temperature. Results from the use of spectroscopic techniques show that activated catalysts exhibit three distinguishable acid sites: (i) eight-ring Brønsted sites (high-frequency hydroxyls or HF OH), (ii) six-ring Brønsted sites (low-frequency hydroxyls or LF OH), and (iii) nonframework AlOH sites. The six-ring/LF OH sites desorb ammonia first with increasing temperature and appear to dealuminate before the eight-ring/HF OH sites. Increasing severity of activation results in framework dealumination. Below 450 °C, dealumination occurs primarily at the low-frequency Brønsted site; above 450 °C, dealumination occurs at both sites. Growth of SiOH peaks at 650 °C is consistent with formation of framework defects due to more extensive dealumination. Increased potassium cation content was found to increase zeolite stability toward framework dealumination, resulting in improved catalyst activity. Catalysts activated at 550 °C, containing framework and nonframework acid sites, appear to offer optimal activity and shape selectivity.

Acknowledgment. Many colleagues provided valuable assistance and participated in fruitful technical discussions: E. G. Lutz, R. L. Meyers, J. W. Mitchell, G. E. Parris, D. R. Shoap, and S. J. Weigel (synthesis); C. G. Coe, J. B. Higgins, R. J. Kitzhoffer, M. J. Labuda, and D. A. Terwilliger (characterization). We also thank Air Products and Chemicals, Inc. for permission to publish this work.

References and Notes

(1) Ashina, Y.; Fujita, T.; Fukatsu, M.; Yagi, J. Process for Producing Dimethylamine in Preference to Mono- and Tri-methylamines by Gas-Phase Catalytic Reaction of Ammonia with Methanol. U.S. Patent 4,582,936, April 15, 1986.

(2) Corbin, D. R.; Schwarz, S.; Sonnichsen, G. C. *Catal. Today* **1997**, *37*, 71.

(3) Wilhelm, F. C.; Parris, G. E.; Aufdembrink, B. A.; Gaffney, T. R. Preparation of Methylamines using Shape Selective Chabazites. U.S. Patent 5,399,769, March 21, 1995.

(4) Ilao, M. C.; Yamamoto, H.; Segawa, K. *J. Catal.* **1996**, *161*, 20.

(5) Veefkind, V. A.; Lercher, J. A. *J. Catal.* **1998**, *180*, 258.

(6) Grundling, C.; EderMirth, G.; Lercher, J. A. *Res. Chem, Intermed.* **1997**, *23*, 25.

(7) Segawa, K.; Ilao, M. C. *Stud. Surf. Sci. Catal.* **1997**, *105B*, 1219.

(8) Szostak, R. *Handbook of Molecular Sieves − Structures*; Van Nostrand Reinhold: New York, 1992; pp. 117−124.

(9) Smith, L.; Cheetham A. K.; Marchese, L.; Thomas, J. M.; Wright, P. A.; Chen, J. *Catal. Lett.* **1996**, *41*, 13.

(10) Smith, L. J.; Davidson, A.; Cheetham, A. K. *Catal. Lett.* **1997**, *49*, 143.

(11) Smith, L. J.; Eckert, H.; Cheetham, A. K. *Chem. Mater.* **2001**, *13*, 385.

(12) Smith, L. J.; Eckert, H.; Cheetham, A. K. *J. Am. Chem. Soc.* **2000**, *122*, 1700.

(13) Vollmer, J. M.; Stefanovich, E. V.; Truong, T. N. *J. Phys. Chem. B* **1999**, *103*, 9415.

(14) Janchen, J.; van Wolput, J. H. M. C.; van de Ven, L. J. M.; de Haan, J. W.; van Santen, R. A. *Catal. Lett.* **1996**, *39*, 147.

(15) Jacobs, P. A.; Mortier, W. J. *Zeolites* **1982**, *2*, 226.

(16) Jeanvoine, Y.; Angyan, J. G.; Kresse, G.; Hafner, J. *J. Phys. Chem. B* **1998**, *102*, 5573.

(17) Kotrel, S.; Lunsford, J. H.; Knoziger, H. *J. Phys. Chem. B* **2001**, *105*, 3917.

(18) Sierka, M.; Eichler, U.; Datka, J.; Sauer, J. *J. Phys. Chem. B* **1998**, *102*, 6397.

(19) Hegde, S. G.; Kumar, R.; Bhatt, R. N.; Ratnasamy, P. *Zeolites* **1989**, *9*, 231.

(20) Cairon, O.; Chavreau, T.; Lavalley, J. C. *J. Chem. Soc., Faraday Trans.* **1998**, *94*, 3039.

(21) Thrush, K. A.; Kuznicki, S. M. *J. Chem. Soc., Faraday Trans.* **1991**, *87*, 1031.

(22) Meissner, H.; Kosslick, H.; Lohse, U.; Parlitz, B.; Tuan, V.-A. *J. Phys. Chem.* **1993**, *97*, 9741.

(23) Sauer, J.; Schröder, K.-P.; Termath, V. *Collect. Czech. Chem. Commun.* **1998**, *63*, 1394.

(24) White, J. L.; Beck, L. W.; Haw, J. F. *J. Am. Chem. Soc.* **1992**, *114*, 6182.

(25) Haw, J. F.; Hall, M. B.; Alvarado-Swaisgood, A. E.; Munson, E. J.; Lin, Z.; Beck, L. W.; Howard, T. *J. Am. Chem. Soc.* **1994**, *116*, 7308.

(26) Beck, L. W.; White, J. L.; Haw, J. F. *J. Am. Chem. Soc.* **1994**, *116*, 9657.

(27) Baba, T.; Ono, Y. *Appl. Catal. A* **1999**, *181*, 227.

(28) Afanassyev, I. S.; Moroz, N. K.; Belitsky, I. A. *J. Phys. Chem. B* **2000**, *104*, 6804.

(29) Haw, J. F. *Phys. Chem. Chem. Phys.* **2002**, *4*, 5431.

(30) Coe, C. G.; Gaffney, T. R.; Srinivasan, R. S. Chabazite for Gas Separation. U.S. Patent, 4,925,460, July 20, 1989.

(31) Engelhardt, G.; Michel, D. *High-Resolution Solid-State NMR of Silicates and Zeolites*; John Wiley & Sons: Rochester, NY, 1987.

(32) Koningsberger, D.; Miller, J. *Stud. Surf. Sci. Catal.* **1996**, *101*, 841.

(33) Beyer, H. K.; Jacobs, P. A.; Uytterhoeven, J. B.; Till, F. *J. Chem. Soc., Faraday Trans. I* **1977**, *73*, 1111.